1-1-2012

Free-standing single-walled carbon nanotube/SnO2 anode paper for flexible lithium-ion batteries

Lukman Noerochim
University of Wollongong, ln865@uowmail.edu.au

Jia-Zhao Wang
University of Wollongong, jiazhao@uow.edu.au

Shulei Chou
University of Wollongong, shulei@uow.edu.au

David Wexler
University of Wollongong, david_wexler@uow.edu.au

Free-standing single-walled carbon nanotube/SnO2 anode paper for flexible lithium-ion batteries

Abstract

Free-standingsingle-walledcarbonnanotube/SnO_2 (SWCNT/SnO_2) anodepaper was prepared by vacuum filtration of SWCNT/SnO_2 hybrid material which was synthesized by the polyol method. From field emission scanning electron microscopy and transmission electron microscopy, the CNTs form a three-dimensional nanoporous network, in which ultra-fine SnO_2 nanoparticles, which had crystallite sizes of less than 5 nm, were distributed, predominately as groups of nanoparticles on the surfaces of singlewalled CNT bundles. Electrochemical measurements demonstrated that the anodepaper with 34 wt.% SnO_2 had excellent cyclic retention, with the high specific capacity of 454 mAh g^{-1} beyond 100 cycles at a current density of 25 mA g^{-1}, much higher than that of the corresponding pristine CNT paper. The SWCNTs could act as a flexible mechanical support for strain release, offering an efficient electrically conducting channel, while the nanosized SnO_2 provides the high capacity. The SWCNT/SnO_2 flexible electrodes can be bent to extremely small radii of curvature and still function well, despite a marginal decrease in the conductivity of the cell. The electrochemical response is maintained in the initial and further cycling process. Such capabilities demonstrate that this model hold great promise for applications requiring flexible and bendable Li-ion batteries.

Keywords

walled, single, standing, ion, lithium, flexible, paper, free, anode, batteries, sno2, nanotube, carbon

Disciplines

Engineering | Physical Sciences and Mathematics

Publication Details

Noerochim, L, Wang, J, Chou, S & Wexler, D (2012), Free-standing single-walled carbon nanotube/SnO2 anode paper for flexible lithium-ion batteries, Carbon, 50(3), pp. 1289-1297.

Free-Standing Single-Walled Carbon Nanotube/SnO_2 Anode Paper for Flexible Lithium-Ion Batteries

Lukman Noerochim[a,b*], Jia-Zhao Wang[a], Shu-Lei Chou[a], David Wexler[c], and Hua-Kun Liu[a]

[a]Institute for Superconducting and Electronic Materials, ARC Centre of Excellence for Electromaterials Science, University of Wollongong, NSW 2522, Australia

[b]Department of Material and Metallurgy, Sepuluh Nopember Institute of Technology Sepuluh Nopember, Surabaya 60111, Indonesia

[c]School of Mechanical, Materials and Mechatronic Engineering University of Wollongong, NSW 2522, Australia

[*] Corresponding author : Fax: +61 2 4221 5731, Phone: +61 2 42981494, E-mail address: ln865@uow.edu.au (Lukman Noerochim)

Abstract

Free-standing single-walled carbon nanotube/SnO_2 (SWCNT/SnO_2) anode paper was prepared by vacuum filtration of SWCNT/SnO_2 hybrid material which was synthesized by the polyol method. From field emission scanning electron microscopy and transmission electron microscopy, the CNTs form a three-dimensional nanoporous network, with ultra-fine SnO_2 nanoparticles, which had crystallite sizes of less than 5 nm, were distributed, predominately, as groups of nanoparticles on the surfaces of parallel packets or bunches of single walled CNTs. Electrochemical measurements demonstrated that the anode paper with 31 wt.% of SnO_2 had excellent cyclic retention, with the high specific capacity of 454 mAh g^{-1} beyond 100 cycles at a current density of 25 mA g^{-1}, much higher than that of the corresponding pristine CNT paper. The SWCNTs could act as a flexible mechanical support for strain release, offering an efficient electrically conducting channel, while the nanosized SnO_2 provides the high capacity. The SWCNT/SnO_2 flexible electrodes can be bent to extremely small radii of curvature, and still function well, despite a marginal decrease the conductivity of the cell. After bending, the conductivity of the cell is 4.8×10^{-4} $S \cdot m^{-1}$, which is slightly lower than that of the cell that was no subjected to bending (5.2×10^{-4} $S \cdot m^{-1}$). The electrochemical response is maintained in the initial and further cycling process. Such capabilities demonstrate this model hold great promise for application requiring flexible and bendable Li-ion batteries.

1. Introduction

There has been more interest recently in flexible and bendable energy storage devices, especially in the field of lithium ion batteries [1-3]. Recent advanced technology in various types of soft portable electronic equipment, such as roll-up displays, wearable devices, and implanted medical devices, requires development of flexible batteries as their power sources. Active radio-frequency identification tags and integrated circuit smart cards also require bendable or flexible batteries for operation in daily use [4, 5]. Typically, lithium batteries consist of a positive electrode and a negative electrode spaced by a separator, which is soaked in an electrolyte solution [6]. Each electrode is formed from a metal substrate that is coated with a mixture of an active material, an electrical conductor, a binder, and a solvent. This type of electrode is not suitable for flexible or bendable batteries, because a metal substrate is used to support the active materials. The active material layer will be damaged or peeled off from the substrate if it is bent. Therefore, the development of free-standing flexible electrode materials is important for flexible and bendable energy storage devices. Recent reports show that paper-like material could be adopted as a key element for application in a flexible lithium rechargeable battery, by embedding it with aligned carbon nanotube (CNT) electrode or integrating it with CNT film into a single sheet of paper through a lamination process [7, 8]. Flexible electrode based on free-standing graphene paper also has been reported by Gwon et al. [9].

Single wall carbon nanotubes (SWCNT) are a promising option for lithium ion batteries due to their one-dimensional structure with high length-to-diameter ratio, combined with high porosity and high surface area [10, 11]. In addition, the outstanding physical properties of SWCNTs, such as high theoretical tensile strength, high electrical conductivity, and high flexibility, make SWCNTs potentially useful for producing flexible and bendable free-standing electrodes [12, 13]. Although SWCNTs have several advantages, their practical capacity based free-standing electrode materials, is still low,

less than 200 mAh g^{-1} after 100 cycles [14, 15]. SWCNTs are formed when a graphene sheet is folded to form a cylinder. These cylinders usually aggregate into bundles, which consist of SWCNTs held together by van der Waals forces [16]. These bundles are expected to display a higher capability for intercalating lithium atoms and consequently higher energy storage capacity. In the ideal case, this gives enhanced anode stoichiometry of LiC_2 [17]. The superior battery performance of SWCNTs depends on the ability of lithium ions to enter and leave the nanotube interior at a reasonable rate. This rate can be improved if the lithium ions reach the interior through topological defects on the side walls and open ends. As a matter of fact, in the experiments carried out by Gao et al. [18], the intercalation density was improved up to $Li_{2.6}C_6$ after ball milling, suggesting that the ball-milling process creates defects and breaks the nanotubes, allowing the lithium ions to intercalate inside the nanotubes. However, in this work, we have tried to improve the practical capacity of SWCNTs by hybridizing an electrochemically active second phase with higher capacity on the surface of the SWCNTs by the reflux process.

Tin dioxide is one of the most promising candidates as a second electrochemically active phase to incorporate into carbon-based free-standing electrode for higher specific capacity, due to its own higher specific capacity (781 mAh g^{-1}) [19, 20] and the environmental friendliness of its raw material processing [21]. However, anodes of such high capacity usually suffer severe capacity fading, stemming from both the quick aggregation of tin particles and the huge volume change (over 300%) during Li^+ insertion/extraction cycles, which causes pulverization of the anodes and electrical detachment of active materials [22, 23]. Reducing the material's size down to the nanoscale and dispersing the material into mesoporous structures have proved very effective in solving these problems in similar systems [24-26]. There have already been some reports of applying inorganic – CNT composites as high-capacity anodes for lithium-

ion batteries (LIBs), but all of these composites were prepared using CNTs as collectors for sediments, so carbon black and polymer binders had to be used to lower the resistance and hold the electrodes together [24, 27, 28]. In contrast, self-supported SWCNT films have been demonstrated to be very attractive candidates for free-standing (not needing any current collectors) and binder-free anodes in LIBs. These will not only significantly improve the specific mass capacity of practical LIBs, but also lower the manufacturing costs. In addition, mesoporous structures of free-standing SWCNT film should be able to effectively accommodate huge volume changes, thereby significantly improving the cycling performance of high-capacity electrodes. Zhang's group has reported binder-free, cross-stacked carbon nanotube sheets with uniformly loaded SnO_2 nanoparticles [29]. Although the composite sheets showed high electrochemical performance with 100 % capacity retention for at least 65 cycles, the synthesis method is quite complicated and time consuming.

In our present work, free-standing SWCNT/SnO_2 anode paper was prepared by a two-step fabrication method. The anode paper shows several advantages. First, SWCNTs can act as a flexible and highly conductive matrix, which can not only accommodate the large volume changes that accompany charge/discharge in tin dioxide, but also provides good contact for the SnO_2-based materials. Second, the deposited SnO_2 can improve the total specific capacity of the SWCNT paper. Finally, the binder-free nature of the anode paper also contributes to the low cost and environmental friendliness of the whole electrode fabrication process.

2. Experimental

2.1 Preparation of SWCNT/ SnO_2 hybrid material

The SWCNT/SnO_2 hybrid material was prepared in the molar ratio of Sn : C of 0.3 : 1. $SnCl_2 \cdot 2H_2O$ (98 %, Sigma-Aldrich) was first dissolved in 50 ml of diethylene glycol (DEG, Fluka), then mixed with SWCNTs (Carbon Nanotechnologies Incorporated (CNI), USA, carbon > 90 %, trace metal basis) by ultrasonication for 1 hour. Subsequently, the solution was placed in a round-bottomed flask. The solution was heated and kept under reflux conditions at 195 ^{o}C for 4 hours with vigorous stirring in air. During the natural cooling process, the magnetic stirring was continued. The resulting products then were washed with acetone several times and collected by centrifuge at 4400 rpm. Finally, the samples were dried at 80 ^{o}C overnight in a vacuum oven.

2.2 Preparation of free-standing SWCNT/ SnO_2 paper

To make a uniform paper, a vacuum filtration technique was adopted [30] with some modifications in our group [14, 15], such as using a 3-piece filter funnel (Whatman). In a typical procedure, 20 mg of SWCNT/SnO_2 hybrid material was dispersed into 1 wt.% of Triton X-100 surfactant (Sigma-Aldrich) in 50 mL of distilled water. The suspension was then ultrasonically agitated using a probe sonicator for 30 min. The as-prepared suspension was poured into the funnel and filtered through a porous polyvinylidene fluoride (PVDF) membrane (Millipore, 0.22 μm pore size, 47 mm in diameter) by positive pressure from the vacuum pump. Since the solvent could pass through the pores of the membrane, the SWCNT/SnO_2 hybrid was trapped on the membrane surface, forming a dark mat. The resultant mat was then washed twice using distilled water, followed by ethanol to remove any remaining surfactant. The mat was allowed to dry overnight at room temperature. Finally, the mat was peeled off from the PVDF membrane, and a SWCNT/SnO_2 paper was obtained. To obtain highly crystalline SnO_2, the paper was heated

at 300 ^{o}C for 30 minutes in air. For comparison, pure free-standing SWCNT paper was also prepared using the same method.

2.3 Physical characterization

Phase analysis was carried out by powder x-ray diffraction (XRD) using a GBC MMA X-ray generator and diffractometer with Cu Kα radiation at a scanning rate of 5^{o} min^{-1} over the 2θ angle range from 10^{o} to 80^{o}. Raman spectroscopy was performed using a JOBIN YVON HR800 Confocal Raman system with 632.8 nm diode laser excitation on a 300 lines mm^{-1} grating at room temperature. The Raman spectra were recorded in the range of 150 – 2000 cm^{-1}. The morphology of the free-standing SWCNT/SnO_2 electrode was investigated by field emission scanning electron microscopy (FE-SEM, JEOL 7500, operated at an acceleration voltage of 1.5 kV), transmission electron microscopy (TEM, JEOL EM 2010), and thermogravimetric analysis (TGA) (Mettler Toledo TGA/DSC 1) for determination of SnO_2 content. TEM samples of the anode paper were prepared by removing a small piece of the paper and mounting it on a folding copper mesh oyster grid.

2.4 Electrochemical measurements

Square model electrodes were cut off from the obtained free-standing paper. The electrodes were then dried at 120 ^{o}C overnight in a vacuum oven. To test the electrochemical performance, charge-discharge in the voltage range of 0.01 - 2 V at constant current density of 25 mA g^{-1} and cyclic voltammetry (CV) at the scan rate of 0.05 mV s^{-1} were performed using a Land battery tester and a CHI 660b electrochemistry workstation, respectively. Electrochemical impedance spectroscopy (EIS) measurements were carried out on the samples with a PARSTAT 2273, using a sine wave of 10 mV

amplitude over a frequency range of 100 kHz – 0.01 Hz. The electrochemical cells (CR 2032 coin-type cells and flexible bendable cells), containing SWCNT/SnO_2 as the working electrode, Li foil as the counter electrode and reference electrode, and a porous polypropylene film as separator, were assembled in an argon gas filled glove box (Mbraun, Germany). The electrolyte was 1 M $LiPF_6$ in a 1 : 2 (v/v) mixture of ethylene carbonate (EC) and diethyl carbonate (DEC).

3. Results and discussion

Figure 1(a) shows the XRD patterns for SWCNTs purchased from CNI, Inc. USA and the SWCNT/SnO_2 paper synthesized by the polyol method. The diffraction peaks of the SWCNT/SnO_2 are consistent with the rutile phase of SnO_2 (JCPDS- No 41-1445), which belongs to space group (SG) $P4_2/mnm$; the individual sets of planes are indexed in the figure. The additional diffraction lines at 2θ of 23° and 44° correspond to the characteristic peaks of SWCNTs. The broad peak of the (0 0 2) diffraction of SWCNT indicates the typical random arrangement of carbon nanotubes, with a $d_{0\,0\,2}$ of 0.38 nm calculated according to Bragg's equation. The peaks of the SWCNT/SnO_2 samples are broad as well, indicating their nanocrystalline nature. The approximate crystallite size of SnO_2 phase in the hybrid was estimated to be around 1.7 nm using the Debye-Scherrer equation applied to the (1 1 0) peak using Traces software, where the Si standard (2 2 0) peak is used as the full-width half-maximum (FWHM) standard.

For quantifying the amount of SnO_2 in the hybrid, TGA was carried out in air. The sample was heated from 25 to 900 °C at a rate of 10 °C min^{-1}. Figure 1(b) shows the TGA curve for the SWCNT/SnO_2 hybrid along with those of the SnO_2 and SWCNT powders. It can be seen that the bare SnO_2 powder remains thermally stable, while the SWCNT/SnO_2 hybrid starts to decompose slowly in air at temperatures above 100 °C, with the SWCNTs

finally burning out at about 600 ^{o}C. Since the bare SnO_2 powder remains stable in this temperature range, any weight change corresponds to the oxidation of SWCNTs. Therefore, the change in weight before and after the oxidation of SWCNTs can be translated into the amount of SnO_2 in the SWCNT/SnO_2 hybrid. With the use of this method, the approximate amount of SnO_2 can be estimated by first subtracting the residual amount of impurities contained in the as-purchased SWCNTs (see detail in Supporting Information). Therefore, the final amount of SnO_2 is approximately 31 wt.%.

Figure 1(c) shows Raman spectra of the pristine SWCNTs, SnO_2, and SWCNT/SnO_2. The Raman spectra of SWCNTs exhibit two main groups of bands whose relative intensities and peak positions vary with excitation wavelength. In the first group, at low wave numbers between 150 and 300 cm^{-1}, one finds the bands associated with radial breathing vibration modes (RBMs), whose peak positions are related to the tube diameter *(d)* through a relationship of the type ν_{RBM} (cm^{-1}) = A/*d* (nm) + B, where A and B are constants that are determined experimentally [31, 32]. The second group, consisting of G and D bands, covers the interval from 1000 to 1700 cm^{-1}. The former, peaking at about 1595 cm^{-1} is attributed to the inplane stretching E_{2g} vibration mode, it being also present in the Raman spectrum of other graphitic materials. The G band reveals an asymmetric profile in its lower-energy side. Raman studies published in 2007, describe the G band profile as being formed from two components, G^+ and G^-. The latter, associated with metallic tubes, is strongly dependent on the tube diameters [33]. Band D, whose peak position varies with the excitation wavelength, is associated with a disorder or defect states induced in the graphitic lattices or nanotubes [32]. In the Figure 1(c) typical SWCNT features are observed for the RBM, D and G band Raman peaks at 256, 1310 and 1596 cm^{-1}, respectively. The radial modes present near 256 cm^{-1} can be correlated with the SWCNT diameters. The peaks present for the pure SWCNT sample suggest that the nanotube

diameter in the sample is approximately 0.92 nm. The Raman spectra of the SWCNT/SnO_2 recorded under excitation at 632.8 nm shows the RBM, D and G band decreases. The G band shifts its peak position to 1594 cm^{-1}. Correlating the above characteristics of the Raman spectra of the SWCNT/SnO_2, one can conclude that the carbon nanotubes are destroyed, a process due to a possible reaction with tin dioxide. The annihilation of the nanotubes occurs because the decrease of the RBM band reveals a destruction of the tubular structure of SWCNT. In the tin dioxide range of the Raman spectra of the SWCNT/SnO_2, the three peaks specific of the SnO_2 (inset, Fig. 1(c)) can not be detected due to the relatively low peak intensity of SnO_2 in the SWCNT/SnO_2 hybrid material [34].

FE-SEM images showing cross-sectional and top views of the SWCNTs and SWCNT/SnO_2 paper are presented in Fig. 2. The top-view FE-SEM image reveals that the SWCNTs and SWCNT/SnO_2 paper appear as webs of curved nanotubes, forming strong inter-twined entanglements with a three-dimensional (3D) network structure. Fig. 2(a) shows single and bundled SWCNTs, which have diameters around 10 - 15 nm and are several micrometres in length. The image of the SWCNT/SnO_2 paper shows that some SnO_2 particles are deposited onto the surface of the SWCNTs in selected sites, with particle sizes in the range of 1 - 5 nm, as shown in Fig. 2(b). The cross-sectional FE-SEM images of the SWCNT/SnO_2 paper in Fig. 2(c) and (d) demonstrate that the CNTs form a 3D network with webs of curved nanotubes in dense and well packed layers and that the total thickness of the paper is around 20 μm. The SnO_2 nanoparticles are clearly visible and attached to the SWCNT matrix in selected areas. The inset of Fig. 2(c) shows a photograph of the SWCNT/SnO_2 paper held by tweezers, indicating the good flexibility.

In the case of the SWCNT/SnO_2 sample, the polyol method can typically produce nanosize SnO_2 particles [35]. In order to confirm the presence of SnO_2 nanoparticles in the anode paper, the TEM samples were prepared by removing a small piece of the anode

paper and mounting it onto a folding copper mesh oyster grid. Figure 3 shows TEM images of the SWCNT/SnO_2 sample. The ultra-fine SnO_2 nanoparticles, which had crystallite sizes of less than 5 nm, were distributed, predominately, as groups of nano particles on the surfaces of parallel packets or bunches of single walled CNTs (Fig. 3(a)-(d)). Closer examination revealed the occurrence of isolated, looped and tangled SWCNTs (marked as T in Fig. 3(a), as single tangled CNTs in Fig. 3(b)), and which can be seen by inspection of Fig. 3(c)). It is believed that these features, assisted in the attachment of the SnO_2 nanoparticles to the bunches of SWCNTs. Selected area electron diffraction revealed fine spotty ring patterns of interplanar d_{hkl} -spacings consistent with SnO_2 (inset, Fig. 3(d)). High magnification imaging revealed SnO_2 lattice fringes (inset, Fig. 3(d)) and contrast consistent with the highly tangled nature of many of packets of SWCNTs.

Cyclic voltammetry (CV) measurements were performed to examine the electrochemical properties of the SWCNTs and the SWCNT/SnO_2 paper during the charge-discharge process. The alloying and de-alloying processes of lithium with SnO_2 and SWCNTs were carried out over the potential range of 2.0 – 0.01 V versus Li/Li^+ at a scanning rate of 0.05 mV s^{-1}, as shown in Fig. 4. Basically, the SWCNT reduction process can be arbitrarily divided into two main regions, above and below ~0.65 V vs. Li/Li^+. In the low potential part (below 0.65 V vs. Li/Li^+), mainly Li-ions are intercalated into the graphitic-type layers. Above 0.65 V vs. Li/Li^+, the sharp negative-going peak at 0.65 V vs. Li/Li^+ is attributed to the formation of the solid electrolyte interphase (SEI) layer [36], as shown in Fig. 4(a). The SWCNT sample exhibits a broad SEI formation peak, indicating that the kinetics of the SEI formation is low. An extra peak at 1.2 V is clearly observed for the SWCNT sample and is attributed to the reduction of surface species containing oxygen [15, 37]. The CV curves for the SWCNT/SnO_2 paper clearly indicate an irreversible reaction during the first discharge, with a reduction peak in the range of 1.1 - 1.2 V, as

shown in Fig. 4(b) and (c). Courtney et al. reported that tin dioxide reacts with lithium in a two-step process, as follows:

$$SnO_2 + 4Li^+ + 4e^- \rightarrow Sn + 2Li_2O \quad (1)$$

$$Sn + xLi^+ + xe^- \leftrightarrow Li_xSn, (0 \leq x \leq 4.4) \quad (2)$$

The reduction peak in the range of 0.9 - 1.0 V can be ascribed to the formation of Sn metal in the Li_2O matrix (Eq. 1), which only happens in the first discharge cycle [22, 38-40]. The sharp negative-going peak at 0.65 V vs. Li/Li^+ is attributed to Li ion intercalation into the graphitic-type layer, as in the CV curves of the pristine SWCNTs. Further cycling led to very sharp and almost identical reduction peaks below 0.5 V and an oxidation peak at 0.5 V. These peaks correspond to the reversible formation of Li_xSn alloys ($0 \leq x \leq 4.4$) (Eq. 2) [22, 38-40]. The cycling stability after 5 cycles of the SWCNT/SnO_2 paper seems to be fairly stable, because the high content of SWCNTs in the sample provides a good conductive matrix for SnO_2 and can also alleviate the volume changes in SnO_2 during alloying and de-alloying processes.

Fig. 4(c) and (d) shows the charge and discharge voltage profiles for the SWCNTs and SWCNT/SnO_2 paper, respectively. The voltage for the SWCNT sample dropped rapidly and formed a plateau at about 0.75 V during the first discharge process, which was attributed to the decomposition of the electrolyte (the formation of the SEI film) [18, 41]. Subsequently, the voltage gradually decreased, delivering a sloping discharge curve at about 0.15 V, with specific discharge capacity as high as 1459 mAh g^{-1}, while for the SWCNT/SnO_2 sample, the discharge capacity could reach up to 1851 mAh g^{-1}. In the SWCNT/SnO_2 sample, the position of the first voltage plateau is shifted to between 1.1 - 1.2 V, which corresponds to the formation of Sn metal in the Li_2O matrix [22, 38-40]. In the voltage range of 1.1 - 1.2 V, no wide plateau is present, and it is only observed that the

drop in the potential changes rapidly in the region of 0.5 - 1.25 V, as shown in Fig. 4(d). Moreover, a flat plateau is observed at low potential (< 0.5 V), which is attributed to the formation of Li_xSn, as described in Equation (2). During the charge processes, prominent voltage plateaus appear at about 0.5 V for the SWCNT/SnO_2 sample, which is attributed to the release of lithium ions when the Li_xSn decomposes (Eq. 2). All these data agree with the cathodic and anodic peak potentials in the cyclic voltammograms.

The discharge capacity versus the number of cycles for cells made from the SWCNT and SWCNT/SnO_2 paper is shown in Fig. 5(a). It can be seen that the discharge capacity is maintained above 187 mAh g^{-1} and 454 mAh g^{-1} beyond 100 cycles for SWCNT and SWCNT/SnO_2 paper, respectively. The results show that the discharge specific capacity of the SWCNT/SnO_2 paper is superior to that of the SWCNTs (187 mAh g^{-1}) because SnO_2 nanoparticles as the active second phase contribute to enhancing the capacity performance of the electrode during cycling. It is well known that the capacity loss in SnO_2 is caused by stress-induced material failure arising from the volume changes in charge and discharge cycling processes. However, the SWCNTs in the hybrid sample are useful for keeping the SnO_2 nanoparticles in good electronic contact and conferring the ability to accommodate the volume changes. The excellent electron and ion transfer kinetics associated with CNTs also contributes to the superior electrochemical performance of the SWCNT/SnO_2 by lowering the internal resistance for both electrons and lithium ions, so as to facilitate the de-alloying reaction over the small surface area of the SnO_2 particles [27]. Even though the volume expansion still occurs, the electrode is not pulverized, as is clear from Fig. 5(b). On the other hand, the specially designed free-standing film materials, integrating the active materials and the current collector into the one flexible film, can prevent loss of the electrical contact between the active materials and the substrate, which normally occurs for the conventional electrode [42]. The high rate

capability of the free-standing, binder-free SWCNT/SnO_2 electrode upon cycling is demonstrated in Fig. 5(b). The flexible, binder-free SWCNT/SnO_2 electrode is very stable, with a slight decrease in specific discharge, to about 186 mAh g^{-1}, when cycled at current densities up to 1,200 mA g^{-1}.

Therefore, in order to verify the electronic conductivity of the SWCNT/SnO_2 paper, electrochemical impedance spectroscopy (EIS) measurements were carried out on the SWCNT/SnO_2 sample using a sine wave of 10 mV amplitude over a frequency range of 100 kHz – 0.01 Hz. To achieve stable SEI formation and the percolation of electrolyte through the electrode materials, the impedance measurement was performed after running charge-discharge for 5 cycles and 100 cycles at a discharged potential of 0.5 V vs. Li/Li^+. Fig. 6 shows the Nyquist plots obtained from the SWCNT/SnO_2 samples after the 5^{th} and 100^{th} cycle tests. An equivalent circuit model was constructed to analyze the impedance spectra, as shown in the inset to Fig. 6(a). Table I shows parameters of the equivalent circuit for the SWCNT/SnO_2 sample after fitting the diameter of the semicircular curve. It is found that the size of the depressed semicircle in the middle frequency range for the SWCNT/SnO_2 sample after 5 cycles is lower than for after 100 cycles, revealing lower charge transfer resistance (R_{ct} = 393.98 Ω) in the SWCNT/SnO_2 sample. This indicates that the electronic conductivity of the SWCNT/SnO_2 sample at initial cycling was enhanced due to the SWCNTs and the good dispersion of the tin particles in the surface of these SWCNTs, which protected the particles from agglomeration during the initial cycling process. However, after 100 cycles, the electronic conductivity of the SWCNT/SnO_2 sample appears slightly lower than in the initial cycles due to the formation of agglomerates on a small scale, decreasing the surface area in the interparticle contact of the tin particles with the surface of the SWCNTs [43, 44], as is shown in the FE-SEM image of Fig. 6(b).

Bending-state electrochemical tests on the free-standing electrode were conducted using a flexible and bendable cell, as shown in Fig. 7(a). To understand the electrochemical behaviour of free-standing electrodes under bending, the flexible and bendable cell was tested when it was bent inwards to 180^{o} (Fig. 7(b)). The capacity of the bent cell is slightly lower compared with the cell that was not subjected to bending (Fig. 7(c)). In order to explore the reason, the conductivity of the cell before and after bending was measured by EIS, as shown in Fig. 7(d). The results show that the application of a tensile stress decreased the conductivity of the electrode [45]. After bending, the conductivity of the cell was 4.8×10^{-4} S·m^{-1}, which is slightly lower than that of the unbent cell (5.2×10^{-4} S·m^{-1}). Although the conductivity of the bent cell decreased, the free-standing electrode is still function well. This suggests that the strain associated with the bending radius is not sufficient to physically crack the working electrode and therefore the structure of the free-standing electrode is not significantly altered by bending test.

4. Conclusions

Free-standing SWCNT/SnO_2 anode paper was prepared by vacuum filtration of SWCNT/SnO_2 hybrid material, which was synthesized by the polyol method. In the SWCNT/SnO_2 paper, the CNTs form a 3D nanoporous network structure, with SnO_2 particles deposited onto the surface of the SWCNTs in selected sites. The SWCNT/SnO_2 paper shows high specific discharge capacity, as great as 454 mAh g^{-1} at a current density of 25 mA g^{-1}, and very stable cycling stability up to 100 cycles compared to the pristine SWCNT paper, due to the intrinsic nature of the combination between nanosized SnO_2 as an active second phase to provide high capacity and the CNTs as flexible mechanical support with high electric conductivity. Bending the SWCNT/SnO_2 electrodes to extremely small radii of curvature has a minimal effect upon the electrochemical behaviour, reflecting a small increase in their electrical resistance. Additionally, the electrochemical

performance was not adversely impacted from bending test. These results illustrate the robust nature of free-standing SWCNT/SnO_2 electrodes and their promise for flexible Li-ion batteries.

Acknowledgements

This research was supported by the Australian Research Council (ARC) through ARC Centre of Excellence for Electromaterials Science funding (EC0561616), administered through the University of Wollongong. Many thanks also go to Dr. T. Silver for critical reading of the manuscript.

References:

[1] Hikmet RAM. New lithium-ion polymer battery concept for increased capacity. Journal of Power Sources. 2001;92(1-2):212-20.

[2] Morris RS, Dixon BG, Gennett T, Raffaelle R, Heben MJ. High-energy, rechargeable Li-ion battery based on carbon nanotube technology. Journal of Power Sources. 2004;138(1-2):277-80.

[3] Nam KT, Kim D-W, Yoo PJ, Chiang C-Y, Meethong N, Hammond PT, et al. Virus-Enabled Synthesis and Assembly of Nanowires for Lithium Ion Battery Electrodes. Science. 2006;312(5775):885-8.

[4] Nishide H, Oyaizu K. Materials Science: Toward Flexible Batteries. Science. 2008;319(5864):737-8.

[5] Suga T, Konishi H, Nishide H. Photocrosslinked nitroxide polymer cathode-active materials for application in an organic-based paper battery. Chemical Communications. 2007(17):1730-2.

[6] Wang J-Z, Chou S-L, Chen J, Chew S-Y, Wang G-X, Konstantinov K, et al. Paper-like free-standing polypyrrole and polypyrrole-$LiFePO_4$ composite films for flexible and bendable rechargeable battery. Electrochemistry Communications. 2008;10(11):1781-4.

[7] Hu L, Wu H, La Mantia F, Yang Y, Cui Y. Thin, Flexible Secondary Li-Ion Paper Batteries. ACS Nano. 2010;4(10):5843-8.

[8] Pushparaj VL, Shaijumon MM, Kumar A, Murugesan S, Ci L, Vajtai R, et al. Flexible energy storage devices based on nanocomposite paper. Proceedings of the National Academy of Sciences.2007;104(34):13574-7.

[9] Gwon H, Kim H-S, Lee KU, Seo D-H, Park YC, Lee Y-S, et al. Flexible energy storage devices based on graphene paper. Energy & Environmental Science. 2011;4(4):1277-83.

[10] Iijima S. Helical microtubules of graphitic carbon. Nature. 1991;354(6348):56-8.

[11] Che G, Lakshmi BB, Fisher ER, Martin CR. Carbon nanotubule membranes for electrochemical energy storage and production. Nature. 1998;393(6683):346-9.

[12] Yu M-F, Files BS, Arepalli S, Ruoff RS. Tensile Loading of Ropes of Single Wall Carbon Nanotubes and their Mechanical Properties. Physical Review Letters. 2000;84(24):5552.

[13] Li F, Cheng HM, Bai S, Su G, Dresselhaus MS. Tensile strength of single-walled carbon nanotubes directly measured from their macroscopic ropes. Applied Physics Letters. 2000;77(20):3161-3.

[14] Ng SH, Wang J, Guo ZP, Chen J, Wang GX, Liu HK. Single wall carbon nanotube paper as anode for lithium-ion battery. Electrochimica Acta. 2005;51(1):23-8.

[15] Chew SY, Ng SH, Wang J, Novák P, Krumeich F, Chou SL, et al. Flexible free-standing carbon nanotube films for model lithium-ion batteries. Carbon. 2009;47(13):2976-83.

[16] Hirsch A. Functionalization of Single-Walled Carbon Nanotubes. Angewandte Chemie International Edition. 2002;41(11):1853-9.

[17] Zhao J, Buldum A, Han J, Ping Lu J. First-Principles Study of Li-Intercalated Carbon Nanotube Ropes. Physical Review Letters. 2000;85(8):1706.

[18] Gao B, Kleinhammes A, Tang XP, Bower C, Fleming L, Wu Y, et al. Electrochemical intercalation of single-walled carbon nanotubes with lithium. Chemical Physics Letters. 1999;307(3-4):153-7.

[19] Y. Idota, T. Kubota, A. Matsufuji, Y. Maekawa, Miyasaka T. Tin-Based Amorphous Oxide: A High-Capacity Lithium-Ion-Storage Material. Science. 1997;276:1395 - 7.

[20] H. Li, Q. Wang, L. Shi, Chen L, Huang X. Nanosized SnSb Alloy Pinning on Hard Non-Graphitic Carbon Spherules as Anode Materials for a Li Ion Battery. Chem Mater. 2002;14 103.

[21] Da Deng, Min Gyu Kim, Lee JY, Cho J. Green energy storage materials: Nanostructured TiO_2 and Sn-based anodes for lithium-ion batteries. Energy Environ Sci. 2009;2:818–37.

[22] Courtney IA, Dahn JR. Key Factors Controlling the Reversibility of the Reaction of Lithium with SnO_2 and Sn_2BPO_6 Glass. Journal of The Electrochemical Society. 1997;144(9):2943-8.

[23] Brousse T, Retoux R, Herterich U, Schleich DM. Thin-Film Crystalline SnO[sub 2]-Lithium Electrodes. Journal of The Electrochemical Society. 1998;145(1):1-4.

[24] Wen Z, Wang Q, Zhang Q, Li J. In Situ Growth of Mesoporous SnO_2 on Multiwalled Carbon Nanotubes: A Novel Composite with Porous-Tube Structure as Anode for Lithium Batteries. Advanced Functional Materials. 2007;17(15):2772-8.

[25] Demir-Cakan R, Hu Y-S, Antonietti M, Maier J, Titirici M-M. Facile One-Pot Synthesis of Mesoporous SnO_2 Microspheres via Nanoparticles Assembly and Lithium Storage Properties. Chemistry of Materials. 2008;20(4):1227-9.

[26] Yu Y, Chen CH, Shi Y. A Tin-Based Amorphous Oxide Composite with a Porous, Spherical, Multideck-Cage Morphology as a Highly Reversible Anode Material for Lithium-Ion Batteries. Advanced Materials. 2007;19(7):993-7.

[27] Noerochim L, Wang J-Z, Chou S-L, Li H-J, Liu H-K. SnO2-coated multiwall carbon nanotube composite anode materials for rechargeable lithium-ion batteries. Electrochimica Acta. 2010;56(1):314-20.

[28] Park M-S, Needham SA, Wang G-X, Kang Y-M, Park J-S, Dou S-X, et al. Nanostructured SnSb/Carbon Nanotube Composites Synthesized by Reductive Precipitation for Lithium-Ion Batteries. Chemistry of Materials. 2007;19(10):2406-10.

[29] Zhang HX, Feng C, Zhai YC, Jiang KL, Li QQ, Fan SS. Cross-Stacked Carbon Nanotube Sheets Uniformly Loaded with SnO_2 Nanoparticles: A Novel Binder-Free and High-Capacity Anode Material for Lithium-Ion Batteries. Advanced Materials. 2009;21(22):2299-304.

[30] De Heer WA, Bacsa WS, Chatelain A, Gerfin T, Humphrey-Baker R, Forro L, et al. Aligned carbon nanotube films: Production and optical and electronic properties. Science. 1995;268(5212):845-7.

[31] Jorio A, et al. Characterizing carbon nanotube samples with resonance Raman scattering. New Journal of Physics. 2003;5(1):139.

[32] Dresselhaus MS, Dresselhaus G, Saito R, Jorio A. Raman spectroscopy of carbon nanotubes. Physics Reports. 2005;409(2):47-99.

[33] Piscanec S, Lazzeri M, Robertson J, Ferrari AC, Mauri F. Optical phonons in carbon nanotubes: Kohn anomalies, Peierls distortions, and dynamic effects. Physical Review B. 2007;75(3):035427.

[34] Sun SH, Meng GW, Zhang GX, Gao T, Geng BY, Zhang LD, et al. Raman scattering study of rutile SnO_2 nanobelts synthesized by thermal evaporation of Sn powders. Chemical Physics Letters. 2003;376(1-2):103-7.

[35] Ng SH, dos Santos DI, Chew SY, Wexler D, Wang J, Dou SX, et al. Polyol-mediated synthesis of ultrafine tin oxide nanoparticles for reversible Li-ion storage. Electrochemistry Communications. 2007;9(5):915-9.

[36] Fong R, von Sacken U, Dahn JR. Studies of Lithium Intercalation into Carbons Using Nonaqueous Electrochemical Cells. Journal of The Electrochemical Society. 1990;137(7):2009-13.

[37] Lu W, Chung DDL. Anodic performance of vapor-derived carbon filaments in lithium-ion secondary battery. Carbon. 2001;39(4):493-6.

[38] Yuan L, Guo ZP, Konstantinov K, Wang JZ, Liu HK. In situ fabrication of spherical porous tin oxide via a spray pyrolysis technique. Electrochimica Acta. 2006;51(18):3680-4.

[39] Wang Y, Su F, Lee JY, Zhao XS. Crystalline Carbon Hollow Spheres, Crystalline Carbon-SnO2 Hollow Spheres, and Crystalline SnO_2 Hollow Spheres: Synthesis and Performance in Reversible Li-Ion Storage. Chemistry of Materials. 2006;18(5):1347-53.

[40] Chen Y-J, Zhu C-L, Xue X-Y, Shi X-L, Cao M-S. High capacity and excellent cycling stability of single-walled carbon nanotube/SnO_2 core-shell structures as Li-insertion materials. Applied Physics Letters. 2008;92(22):223101-3.

[41] J.Y. Eom, Kwon HS. Improved lithium insertion/extraction properties of single-walled carbon nanotubes by high-energy ball milling. J Mater Res 2008;23:2458.

[42] Graetz J, Ahn CC, Yazami R, Fultz B. Highly Reversible Lithium Storage in Nanostructured Silicon. Electrochemical and Solid-State Letters. 2003;6(9):A194-A7.

[43] Fan J, Fedkiw PS. Electrochemical impedance spectra of full cells: Relation to capacity and capacity-rate of rechargeable Li cells using $LiCoO_2$, $LiMn_2O_4$, and $LiNiO_2$ cathodes. Journal of Power Sources. 1998;72(2):165-73.

[44] Ng SH, Wang J, Konstantinov K, Wexler D, Chen J, Liu HK. Spray Pyrolyzed PbO-Carbon Nanocomposites as Anode for Lithium-Ion Batteries. Journal of The Electrochemical Society. 2006;153(4):A787-A93.

[45] Cai J, Cizek K, Long B, McAferty K, Campbell CG, Allee DR, et al. Flexible thick-film electrochemical sensors: Impact of mechanical bending and stress on the electrochemical behavior. Sensors and Actuators B: Chemical. 2009;137(1):379-85.

Figure captions

Figure 1

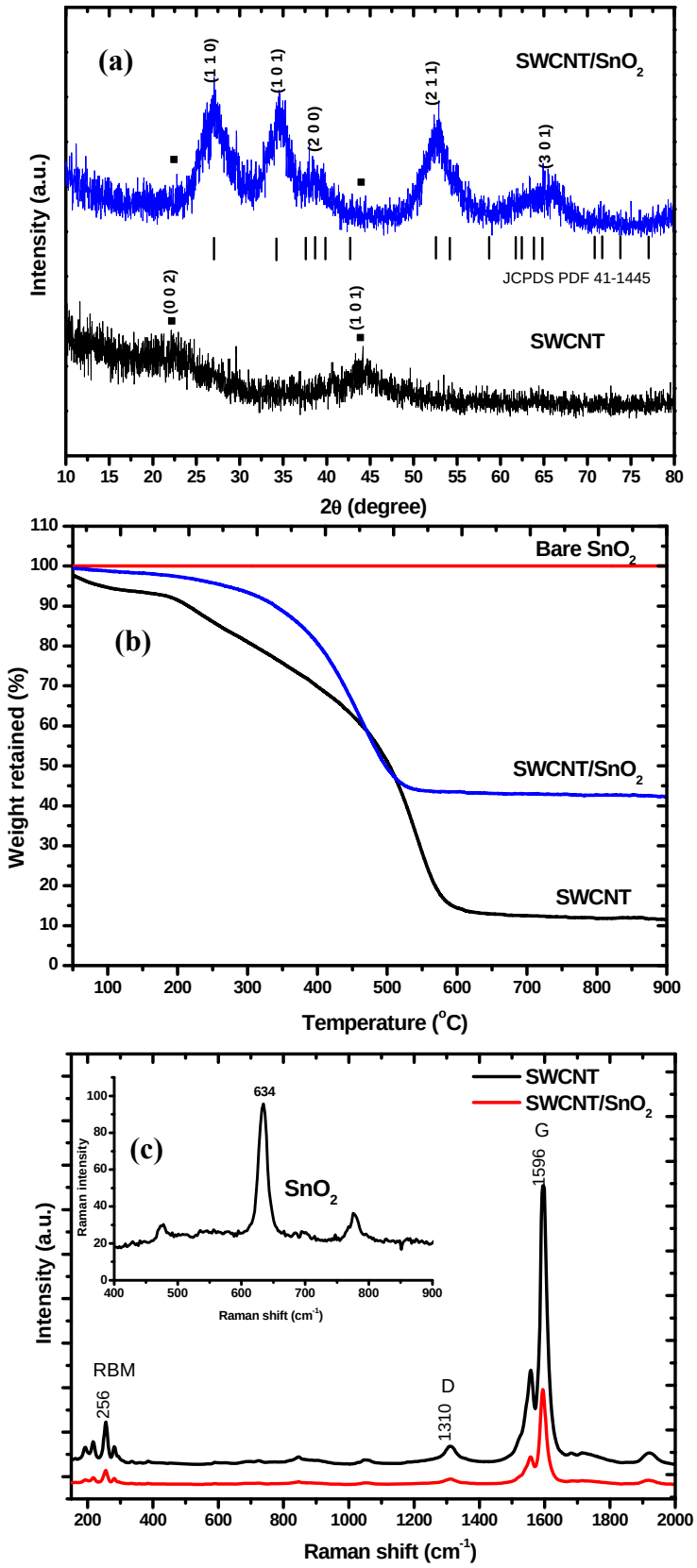
(a)
SWCNT/SnO2
(1 1 0)
(1 0 1)
(2 0 0)
(2 1 1)
(3 0 1)
JCPDS PDF 41-1445
(0 0 2)
(1 0 1)
SWCNT
Intensity (a.u.)
2θ (degree)
(b)
Bare SnO2
SWCNT/SnO2
SWCNT
Weight retained (%)
Temperature (°C)
(c)
SWCNT
SWCNT/SnO2
634
SnO2
Raman intensity
Raman shift (cm-1)
G
1596
RBM
256
D
1310
Intensity (a.u.)
Raman shift (cm-1)

Figure 2

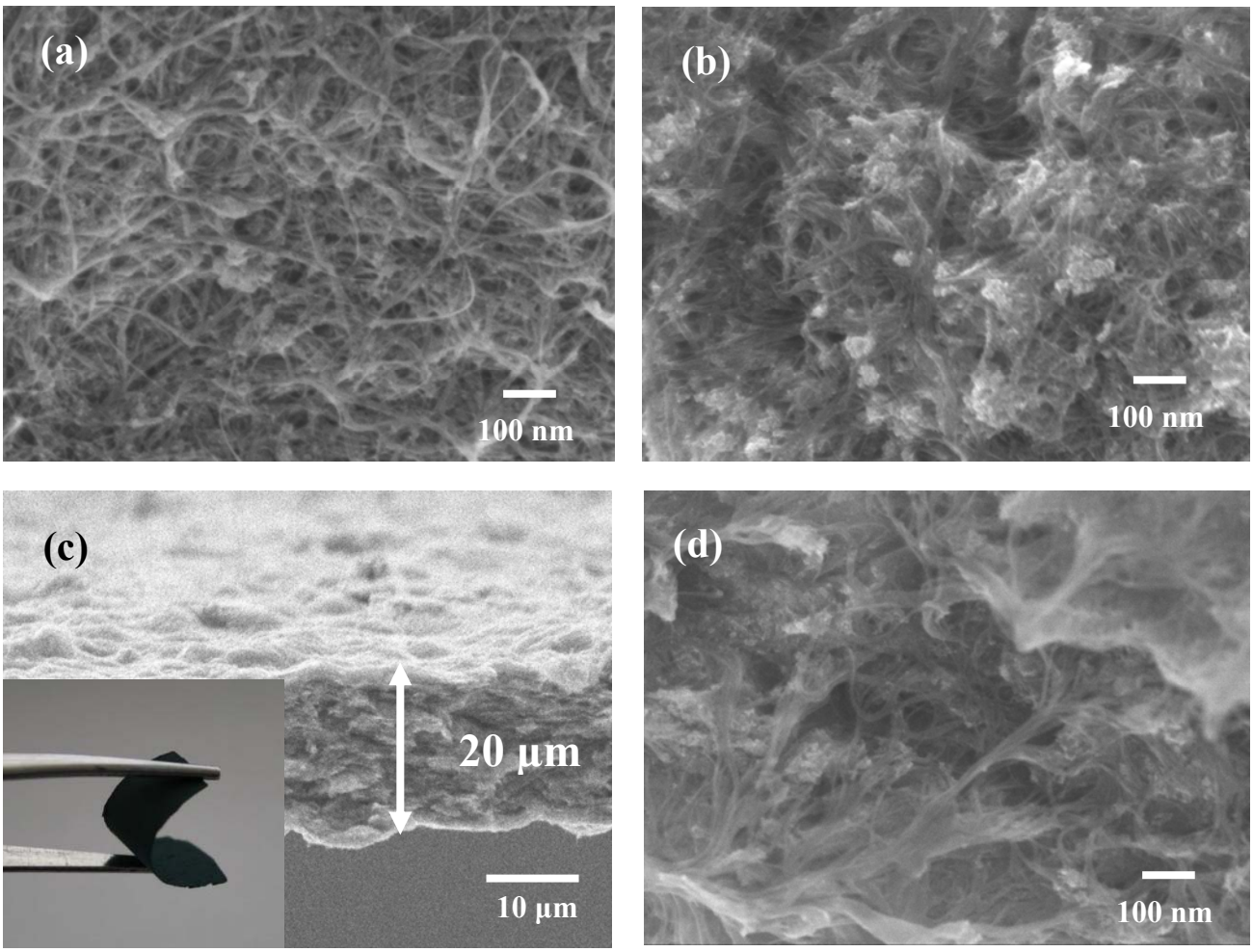

Figure 3

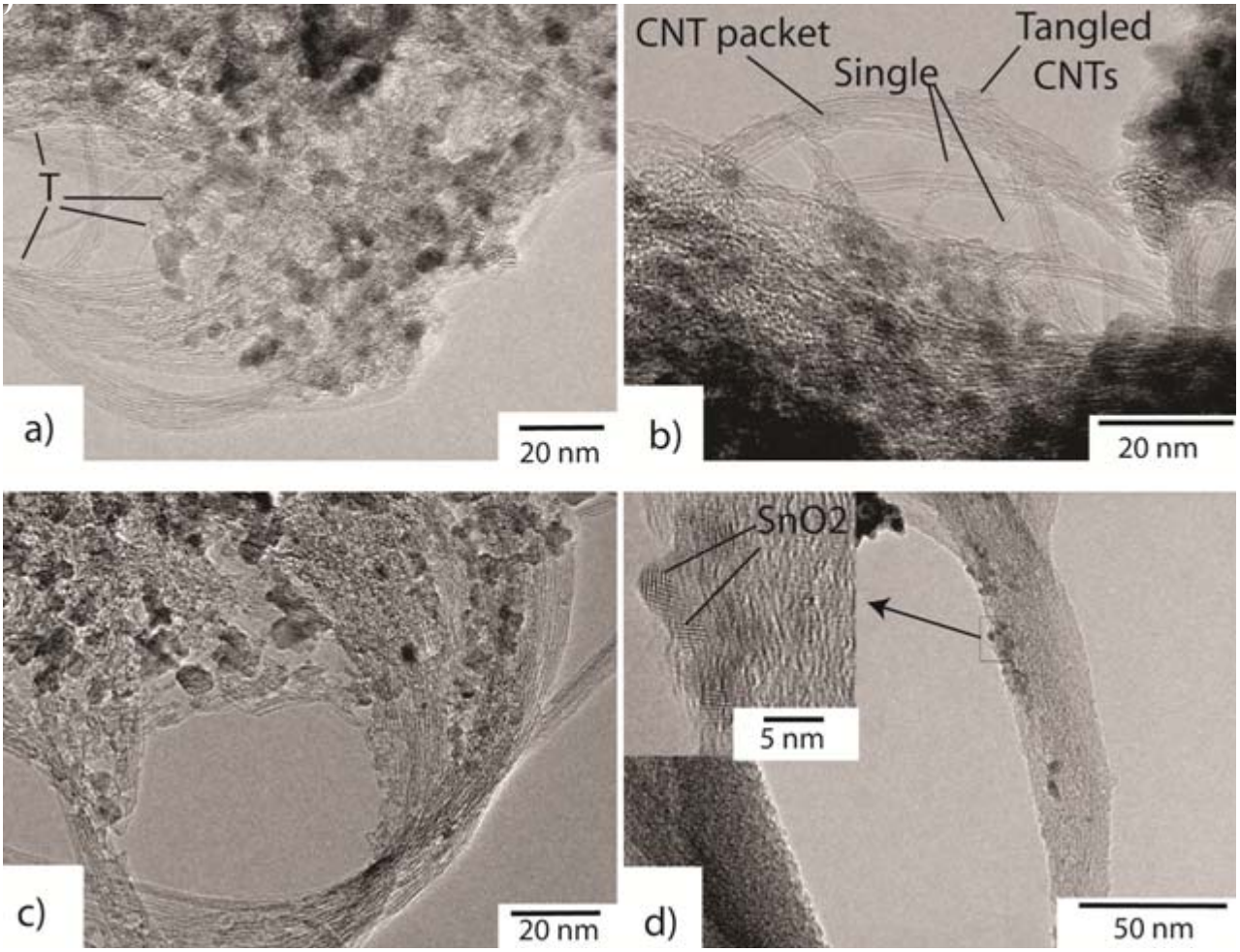
T
a)
20 nm
CNT packet
Single
Tangled
CNTs
b)
20 nm
c)
20 nm
SnO2
5 nm
d)
50 nm

Figure 4

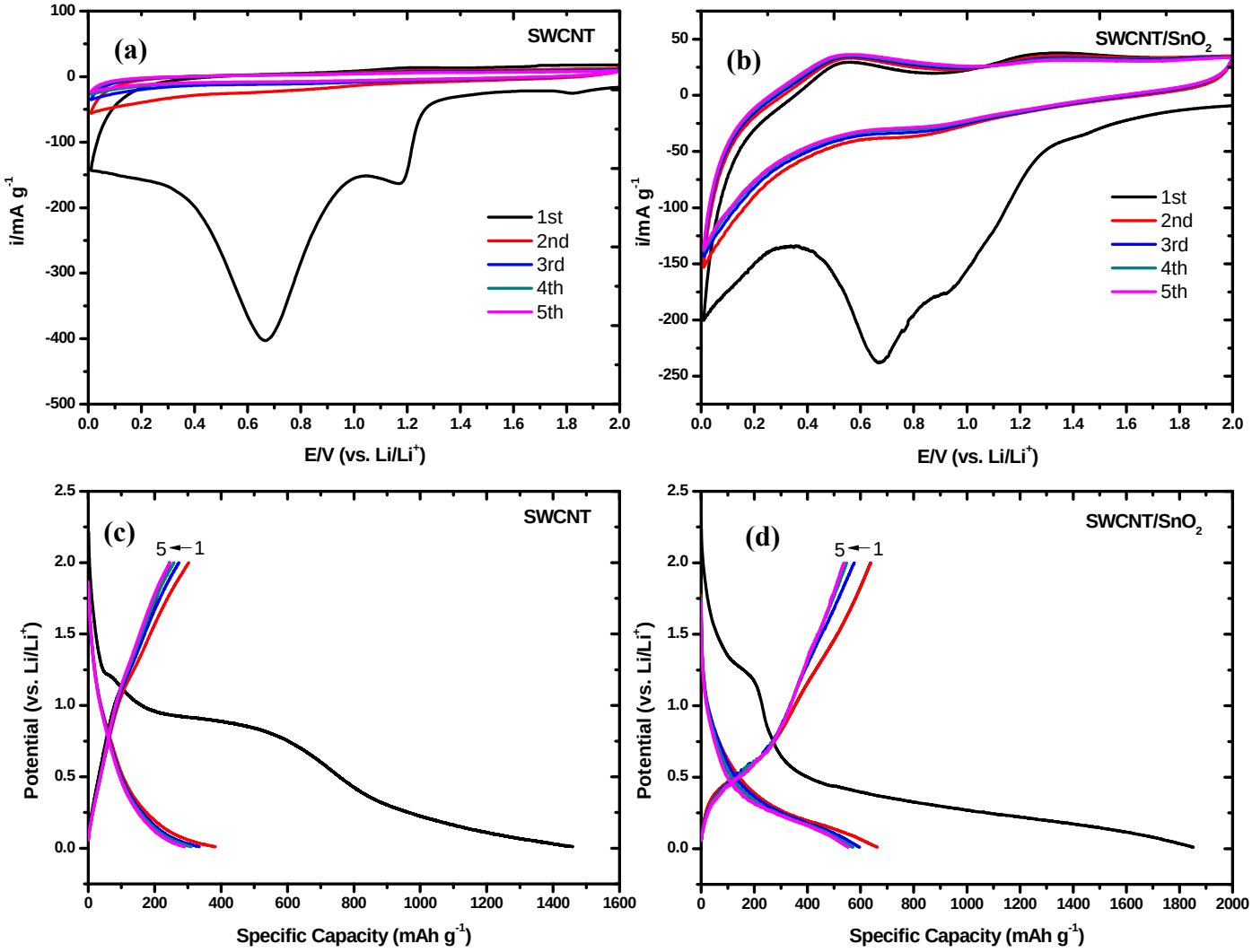
(a)
SWCNT
1st
2nd
3rd
4th
5th
i/mA g-1
E/V (vs. Li/Li+)
(b)
SWCNT/SnO2
1st
2nd
3rd
4th
5th
i/mA g-1
E/V (vs. Li/Li+)
(c)
SWCNT
5←1
Potential (vs. Li/Li+)
Specific Capacity (mAh g-1)
(d)
SWCNT/SnO2
5←1
Potential (vs. Li/Li+)
Specific Capacity (mAh g-1)

Figure 5

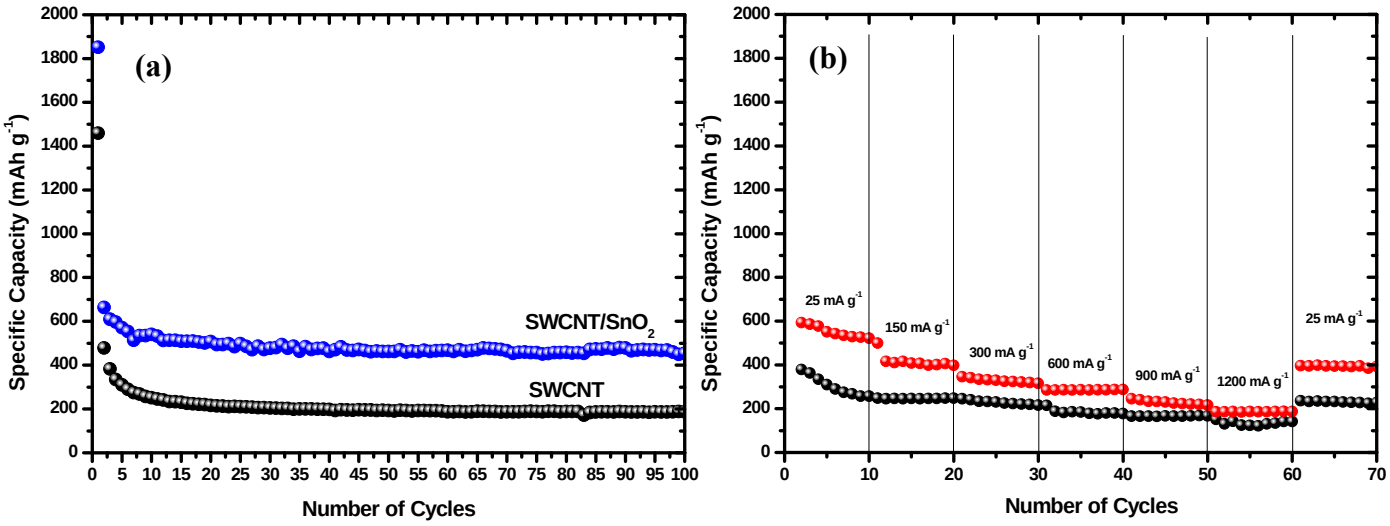
(a)
Specific Capacity (mAh g-1)
Number of Cycles
SWCNT/SnO2
SWCNT
(b)
Specific Capacity (mAh g-1)
Number of Cycles
25 mA g-1
150 mA g-1
300 mA g-1
600 mA g-1
900 mA g-1
1200 mA g-1
25 mA g-1

Figure 6

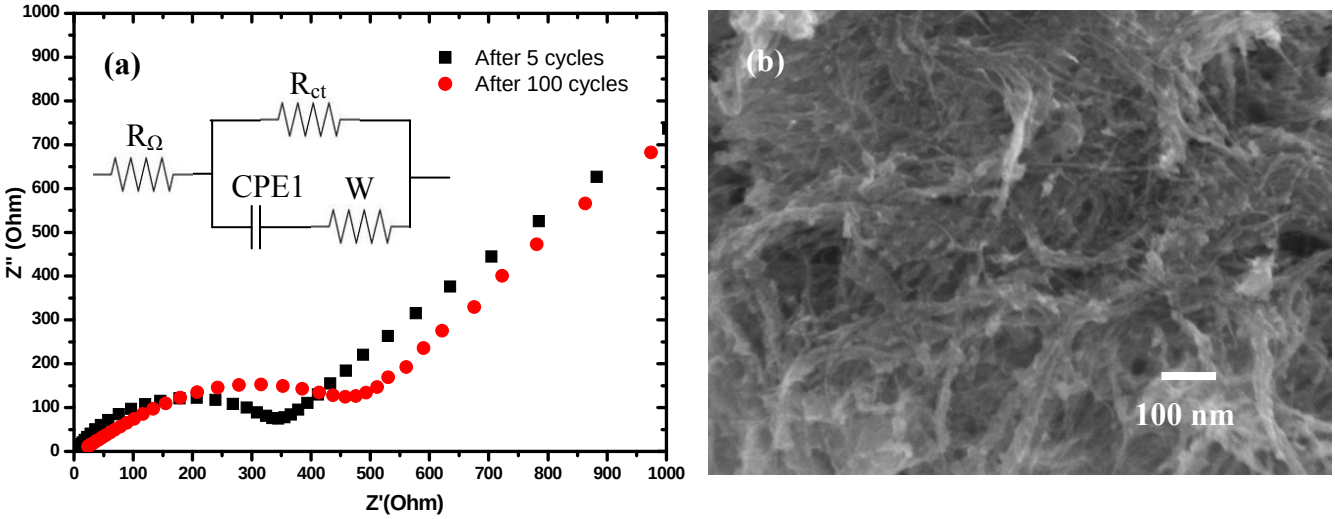
(a)
After 5 cycles
After 100 cycles
R_{ct}
R_{Ω}
CPE1
W
Z'' (Ohm)
Z'(Ohm)
0
100
200
300
400
500
600
700
800
900
1000
(b)
100 nm

Figure 7

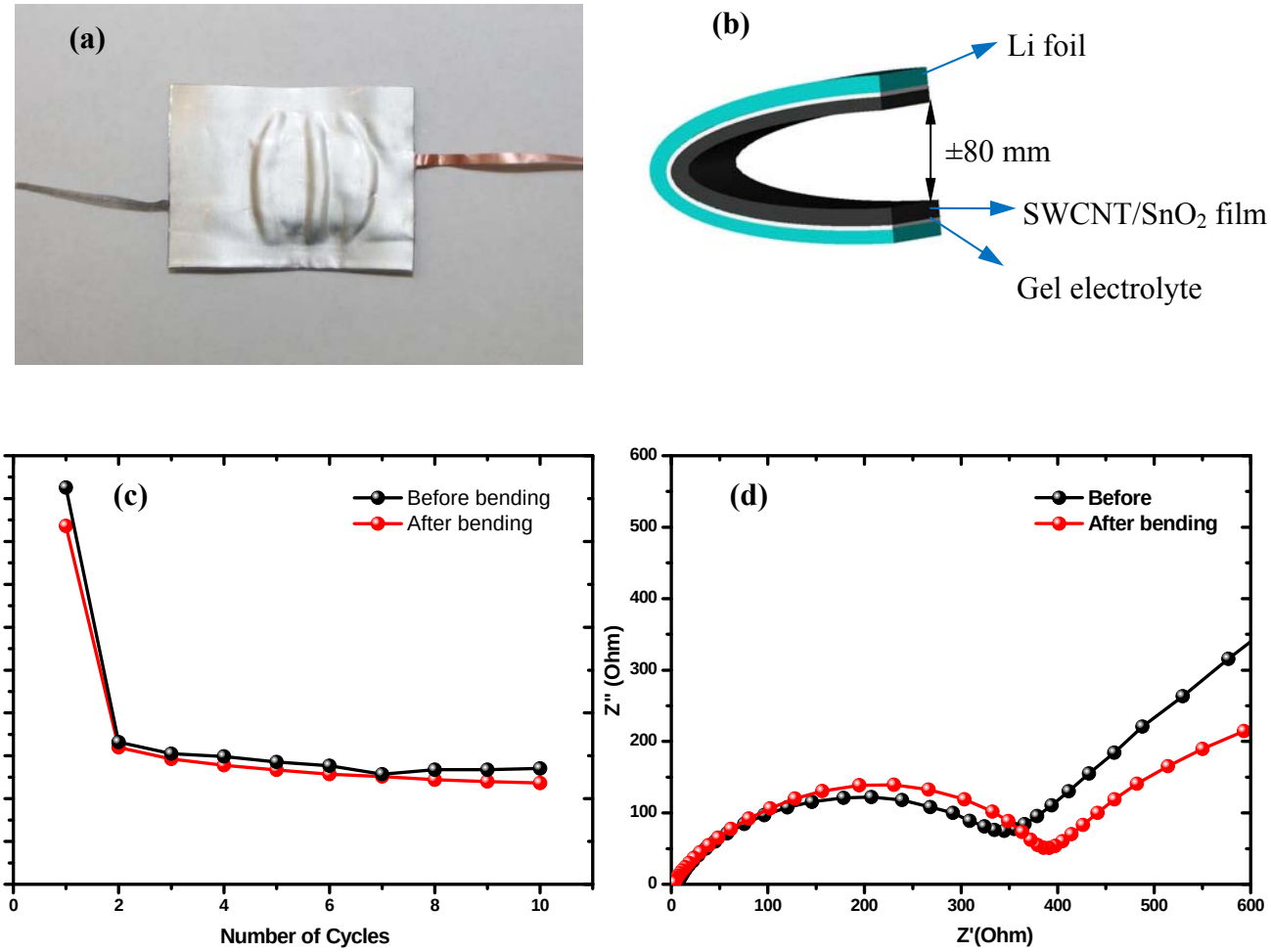
(a)
(b)
Li foil
±80 mm
SWCNT/SnO2 film
Gel electrolyte
(c)
Before bending
After bending
Specific Capacity (mAh g-1)
Number of Cycles
(d)
Before
After bending
Z'' (Ohm)
Z'(Ohm)

Table captions

Table I.

Electrode Materials	Cycles	R_{Ω} (Ω)	R_{ct} (Ω)
SWCNT/SnO_2	5	1.2	393.98
	100	19.76	601.15